Radiat Environ Biophys
DOI 10.1007/s00411-007-0099-y

Description of light ion production cross sections and fluxes on the Mars surface using the QMSFRG model

Francis A. Cucinotta · Myung-Hee Kim · Susana I. Schneider · Donald M. Hassler

Received: 4 October 2006 / Accepted: 24 January 2007

Abstract The atmosphere of Mars significantly attenuates the heavy ion component of the primary galactic cosmic rays (GCR), however, increases the fluence of secondary light ions (neutrons, and hydrogen and helium isotopes) because of particle production processes. We describe results of the quantum multiple scattering fragmentation (QMSFRG) model for the production of light nuclei through the distinct mechanisms of nuclear abrasion and ablation, coalescence, and cluster knockout. The QMSFRG model is shown to be in excellent agreement with available experimental data for nuclear fragmentation cross sections. We use the QMSFRG model and the space radiation transport code, HZETRN to make predictions of the light particle environment on the Martian surface at solar minimum and near maximum. The radiation assessment detector (RAD) experiment will be launched in 2009 as part of the Mars Science Laboratory (MSL). We make predictions of the expected results for time dependent count-rates to be observed by the RAD experiment. Finally, we consider sensitivity assessments of the impact of the Martian atmospheric composition on particle fluxes at the surface.

F. A. Cucinotta (✉) · M.-H. Kim
NASA, Lyndon B. Johnson Space Center,
Houston, TX, USA
e-mail: francis.a.cucinotta@nasa.gov

S. I. Schneider
Penn State University, State College, PA, USA

D. M. Hassler
Southwest Research Institute, Boulder, CO, USA

Introduction

Human beings are scheduled to visit Mars in the 2030 to 2040 time-period. Prior to their arrival an accurate assessment of the radiation environment on the Mars surface is required. Particle flux distributions, which describe particle type (charge and mass), j, kinetic energy, E(MeV/u), and particle directions are necessary for a complete description of radiation fields in space because the use of dose equivalent carries large uncertainties in projecting risk of late effects from galactic cosmic rays (GCR) [1–3]. The primary GCR are well described by empirical models based on extensive measurements [4]. The description of the GCR on the planetary surface of Mars is expected to be more challenging because of larger amount of material ions traverse in the Mars atmosphere and backscatter of neutrons and other light ions from the Mars regolith [5]. The water content near the surface of Mars could play an important role in reducing the low-energy neutron components on Mars [5]. Nuclear fragmentation and energy loss processes are the main physical mechanisms in GCR transport. In this report we briefly summarize a quantum multiple scattering model of nuclear fragmentation (QMSFRG) and describe its extension to incorporate nuclear coalescence as a mechanism of light ion production. The RAD experiment will be launched in 2009 as part of the Mars Surface Lander (MSL). In this report we discuss predictions of the expected results for time dependent count-rates to be observed by RAD experiment on Mars, and evaluate the role of the altitude of a landing site and the atmospheric composition.

Journal : 411 | Dispatch : 8-2-2007 | Pages : 7
Article No. : 99 | LE | TYPESET
MS Code : 99 | CP | DISK

Methods

Quantum fragmentation model

The QMSFRG is a fundamental approach rooted in the multiple scattering series for two heavy ions, which is solved within the impulse and eikonal approximation for the total momentum transfer vector in order to obtain a closed-form solution to the abrasion cross section excitation spectrum [6–10]. For inclusive reactions where a single fragment originating in the projectile is measured, closure is performed on the final target state with a momentum vector denoted $\mathbf{p}_X$ used to represent these states. The reaction is assumed to proceed through the abrasion step producing a pre-fragment, F^* and fireball piece from the projectile-target overlap denoted, R, followed by the ablation step where the final projectile fragment, F is formed after nuclear de-excitation. The total momentum transfer is $\mathbf{q} = \mathbf{p}_T - \mathbf{p}_X$ where $\boldsymbol{p}_T$ is the initial target momentum. The pre-fragment, F^* excitation spectrum following nucleon or alpha particle abrasion was found [7, 8] as an impact parameter dependent convolution of the pre-fragment excitation response for a transition of the pre-fragment core from state n to n' and the project fireball response, averaged over the target ground-state wave function, $|T>$,

$$\frac{\mathrm{d}\sigma}{\mathrm{d}E_{F*}} = <T| \int d^2q d^2b d^2b' \mathrm{e}^{iq(b-b')} P_{n,n'}(b,b',E_{F*}) \times \Lambda_{n,n'}(q,b,b',E_{F*})|T> \quad (1)$$

where b (b') is the impact parameter, and q the momentum transfer. The abrasion response is defined as the quantum matrix elements for the interaction of the projectile fireball, R with the target, T after performing closure over the final fireball states (denoted $|R>$)

$$\Lambda_{n,n'}(q,b,b',E_{F*}) = \int \frac{\mathrm{d}\mathbf{k}_R}{(2\pi)^3} <R'|Q^+_{RT}(b')|R> <R|Q_{RT}(b)|R'>\delta(E_i - E_f) \quad (2)$$

where the Q_{RT} represent the fireball-target profile operator, and $\mathbf{k}_R$ the projectile fireball momentum vector. The abrasion-response represents a complicated many-body operator that is solved by approximation using closure over the target and fireball states for evaluating the pre-fragment distribution. The one-particle abrasion response has been evaluated using the shell model response functions [8, 9]. The pre-fragment excitation is described in terms of the transition matrix

$$P_{n,n'}(b,b',E_{F*}) = <F^*_n|Q^+_{F^*T}(b')|F^*_{n'}> <F^*_{n'}|Q_{F^*T}(b)|F^*_n> \quad (3)$$

where quantum matrix elements for the pre-fragment excitation are evaluated over the many-body profile operators, Q_{F^*T}. In the model a convolution approach is used to derive the multi-nucleon abrasion excitation spectrum from the single-fragmentation term [7, 8]. The resulting excitation spectrum is broad with a shape similar to a log-normal distribution with mean energies from 20 to 30 MeV for one-nucleon removal. The inputs to the model include the energy-dependent two-body t-matrix, density-dependent medium corrections to the nucleon–nucleon, cross sections, and single particle wave functions. These inputs are independent of the fragmentation data being considered.

The de-excitation of the pre-fragments in nuclear ablation is described in a stochastic process using a Master equation for de-excitation by particle emission [9, 10]. If $f_b(E,t)$ is the probability of finding the nuclei b at time t with excitation energy E_b and $P_{b,k}(E)$ be the probability that the nuclei, b will emit ion k with energy E, then the Master equation is

$$\frac{\mathrm{d}f_b(E^*_b,t)}{\mathrm{d}t} = \sum_j \int \mathrm{d}E f_a(E^*_a,t)P_{a,j}(E) - \sum_k \int \mathrm{d}E f_b(E^*_b,t)P_{b,k}(E) \quad (4)$$

The first-term on the right side of Eq. (4) corresponds to gains by decays of ion a emitting ion j to form ion, b, and the second term from losses due to decays of ion b into ion c by emitting ion k where the j (or k) are light-particle emissions (n, p, d, t, h, or α). The probability of finding the nuclei b at time t with E^*_b can be divided into stable and unstable parts depending on the lowest excitation energy of E^*_b, denoted min[S_{bj}],

$$f(E^*_b,t) = g(E^*_b,t) + h(E^*_b,t) \quad (5)$$

where g and h denote the stable and unstable parts of f, respectively. As $t \rightarrow \infty$, we have $h \infty 0$ such that

$$\lim_{t\to\infty} f(E^*_b,t) = g(E^*_b,\infty) \quad (6)$$

The probabilities for a single-step decay of nucleus a, are defined as

Journal : 411 Article No. : 99 MS Code : 99 Dispatch : 8-2-2007 LE CP Pages : 7 TYPESET DISK

$$F_{a,j} = \int_0^{E^* - S_{a,j}} P_{a,j}(E)\mathrm{d}E \quad (7)$$

with a stable daughter nuclei, b formed corresponding to the probability

$$G_{a,j} = \int_{E^* - S_{a,j} - \min[S_{b,k}]}^{E^* - S_{a,j}} P_{a,j}(E)\mathrm{d}E \quad (8)$$

and an unstable daughter nuclei formed with probability

$$H_{a,j} = \int_0^{E^* - S_{a,j} - \min[S_{b,k}]} P_{a,j}(E)\mathrm{d}E \quad (9)$$

These probabilities obey

$$F_{a,j} = G_{a,j} + H_{a,j} \quad (10)$$

and the normalization condition, $\sum_j F_{a,j} = 1$. Because only stable nuclei remain at long times, the differo-integral Eq. (4) is separated using the above definitions as

$$g_b(E_b^*, \infty) = g_b(E_b^*, 0) + \sum_j \int_0^\infty \mathrm{d}t \int \mathrm{d}E f_a(E_b^*, t) P_{a,j}(E) \quad (11)$$

and similarly

$$0 = h_b(E_b^*, 0) + \sum_j \int_0^\infty \mathrm{d}t \int \mathrm{d}E f_a(E_b^*, t) P_{a,j}(E) \quad (12)$$

In evaluating fragmentation cross sections, Eqs. (11) and (12) are solved by iteration up to excitation energies of 200 MeV [9, 10], and using the approximation of Campi and Hufner [11] at higher values. The use of the statistical decay model with accurate nuclear level densities that include nuclear shell structure effects and the use of measured values for the nuclear masses are important for accurately predicting the odd–even effects in the fragment spectrum.

To estimate nuclear coalescence contributions to d, t, h, and α production we consider the momentum distribution for proton (p) and neutron (n) production in the QMSFRG model [10, 12], and apply the usual coalescence model [13], which consists of an A_n-fold folding of the p- and n- distribution to form a light ion of mass number A_n. The n and p production cross sections are then reduced by the appropriate balancing of the cross sections resulting in light nuclei coalescence. In these estimates only the contributions from abrasion momentum distributions is used.

Space radiation transport code

We use the HZETRN code of Wilson et al. [14, 15] in our predictions of the Mars surface. HZETRN solves for the spectrum of heavy ion fragment from projectile and target nuclei in the continuous slowing down and straight-ahead approximations. Integration over the Martian atmospheres is performed as described previously [3]. We have modified the HZETRN code in several ways: First we have extended the ion grid to 190-ions from the earlier 59-ion [13] or 170-ion [16]

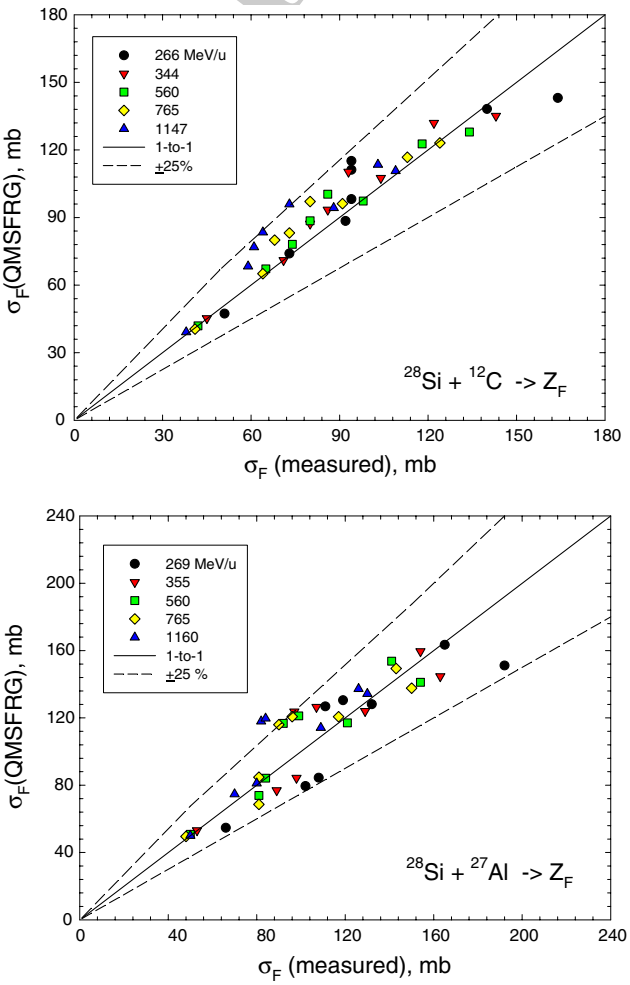

Fig. 1 Comparisons of fragmentation cross sections in QMSFRG model to experimental data [19] for ^{28}Si fragmentation on C and Al targets at several energies. Correlations between model and data are shown for fragments with Z = 13 to 7. Experimental errors are typically less than 10% as reported by Zeitlin et al. [17]

Journal : 411 Dispatch : 8-2-2007 Pages : 7
Article No. : 99 LE TYPESET
MS Code : 99 CP DISK

Table 1 Contributions to light ions production in ^{16}O fragmentation in QMSFRG compared to experiment [18]

Secondary	QMSFRG theory						Experiment
	Abrasion	Coalescence	Cluster KO	E&M Diss	Ablation	Total	
^{16}O + H → Secondary at 2.1 GeV/u							
n	287.3	–	–	0.04	48.3	284.1	–
p	291.4	–	–	0.1	70.3	310.2	–
^{2}H	4.8	29.2	–	–	6.3	40.3	152 ±23
^{3}H	2.3	12.7	–	–	2.3	17.3	55 ± 11
^{3}He	1.2	12.7	–	–	3.4	17.3	50.2 ± 5.7
^{4}He	61.7	6.6	9.5	–	91.1	168.9	221 ± 20
^{16}O + ^{12}C → Secondary at 2.1 GeV/u							
n	2692	–	–	0.8	350.5	2697	–
p	2781	–	–	1.2	465.9	2902	–
^{2}H	232.5	196.3	–	–	30.8	459.6	406 ± 36
^{3}H	17.4	85.3	–	–	37.7	140.4	151 ± 11
^{3}He	7.2	65.3	–	–	11.2	103.7	136 ± 7.6
^{4}He	174.4	44.2	21.0	–	218	457.7	474 ± 42
^{16}O + Cu → Secondary at 2.1 GeV/u							
n	6537	–	–	14.2	590.6	6459	–
p	6889	–	–	21.3	712.8	6941	–
^{2}H	380.8	386.9	–	–	49.7	817.4	682 ± 72
^{3}H	27.1	168.0	–	–	55.2	250.3	–
^{3}He	10.6	168.0	–	–	16.0	194.7	–
^{4}He	256.4	87.1	35.7	–	316.5	695.6	748 ± 80

grids with the ions selected after studying the fragment spectra for most GCR nuclei for primaries of $Z = 1$ to 28. Second we use the QMSFRG data base as described earlier. Finally, we use the primary GCR model of Badhwar et al. [4], but re-distribute the most abundant element used in this work amongst the isotopic composition found for the primary GCR as described in Cucinotta et al. [16].

Results and discussion

We first describe comparison of the QMSFRG model to heavy ion fragmentation cross sections. Our recent publication [16] made extensive comparisons of QMSFRG to experimental cross sections for Ne, Mg, Ar, and Fe. In Fig. 1 we show comparisons of the correlations between QMSFRG and the recent data by Zeitlin et al. [17] for ^{28}Si fragmentation cross sections at several energies for C and Al targets. As in our earlier work, QMSFRG demonstrates good agreement with fragmentation cross sections for projectile fragments as function of target mass and beam energy with more than 85% of the cross sections agreeing to within ±25 of measurements. Light ions are produced by several mechanisms including nuclear abrasion, ablation, coalescence, cluster knockout, and electro-magnetic dissociation. In Table 1 we show contributions for several of these mechanisms for ^{16}O fragmentation on several targets and compare to the experimental data of Olsen et al. [18]. Details on the experiments are considered in these references. Coalescence is predicted to be a dominant mechanism for *d*, *t*, *h*, and α-particle production. Calculations include cluster knockout only for α-particle production and appear to be most important for H and other light targets. The differences between theory and experiment suggest that studies of *d*, *t*, and *h* cluster knockout maybe warranted, especially for target fragmentation data bases, and that improved models of nuclear coalescence are needed.

In Table 2 and Figs. 2 and 3 we show predictions for the Mars surface. Table 2 shows the elemental fluence at solar minimum where the solar modulation parameter, Φ of 428 MV is used [4] and for the year 2010 a modulation parameter of 1,000 MV. The value of 1,000 MV is chosen for the anticipated operation of MSL, which will occur about 1-year before solar maximum. The Mars atmosphere significantly depletes the HZE components, and the $Z = 1, 2$ ions will be the main inducers of biological risk for astronauts occupying the Mars surface. The angular view of RAD will be no more than 90° because of the mass limitations on MSL, and we show results for the complete horizon and a restricted vertical horizon of 60 and 90° in Table 2. The acceptance correction due to the detector viewing angle has a slight dependence on the solar modulation parameter because of the higher contri-

Journal : 411 Dispatch : 8-2-2007 Pages : 7
Article No. : 99 LE TYPESET
MS Code : 99 CP DISK

Table 2 Projections of elemental GCR fluences

Charge group, Z	Fluence, 1/(cm^2 h) all angles	Fluence, 1/(cm^2 h) 90° viewing cone	Fluence, 1/(cm^2 h) 60° viewing cone
For RAD surface operations in 2010 (Φ = 1,000 MV)			
0	13841	4374	2751
1	11576	5756	3817
2	425	288	198
3	3.32	2.30	1.58
4	2.40	1.66	1.14
5	3.23	2.38	1.66
6	7.08	5.40	3.82
7	2.34	1.77	1.25
8	4.46	3.56	2.56
9	0.30	0.23	0.16
10	0.80	0.64	0.46
11	0.31	0.24	0.17
12	0.78	0.64	0.46
13	0.20	0.16	0.12
14–17	0.42	0.35	0.26
18–23	0.23	0.19	0.14
>23	0.18	0.16	0.12
Near solar minimum (Φ = 428 MV)			
0	24779	8131	5127
1	22552	11711	780
2	770	527	364
3	5.94	4.19	2.89
4	4.20	2.96	2.04
5	5.58	4.17	2.93
6	12.09	9.37	6.67
7	3.89	2.99	2.12
8	7.40	5.99	4.34
9	0.48	0.36	0.26
10	1.25	1.01	0.73
11	0.48	0.38	0.27
12	1.19	0.99	0.72
13	0.31	0.25	0.18
14–17	0.96	0.80	0.59
18–23	0.33	0.28	0.20
>23	0.25	0.22	0.17

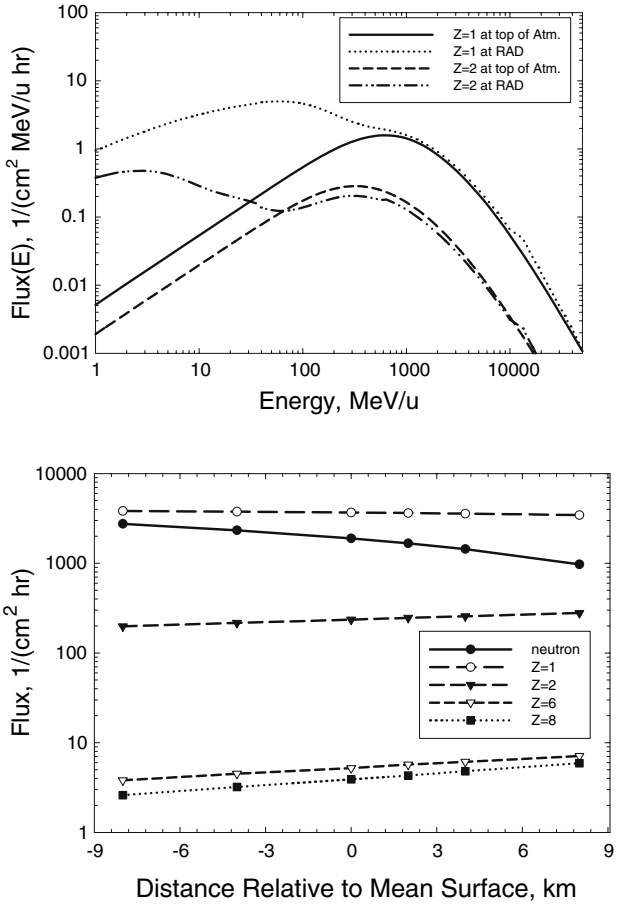

Fig. 2 *Upper panel* shows calculations of the energy spectra of Z = 1 and 2 ions incident on Mars and the average mean altitude projected for 2010 (Φ = 1,000 MV). The *lower panel* shows calculations of the total annual flux of Z = 0, 1, 2, 6, and 8 ions for different mean altitudes on Mars projected for 2010 (Φ = 1,000 MV)

butions of lower energy projectile nuclei at solar minimum. In Fig. 2 we show results for the energy spectra and average fluence of light and heavy ions for different altitudes relative to the mean surface. The shape of the spectrum below 200 MeV/u changes dramatically due to production from GCR heavy ions or target atoms in the atmosphere. At high energies (above a few GeV/u) there is a slight build-up of Z = 1 fragments predicted due to fragmentation of GCR nuclei. We have not included the backward neutron components in these comparisons, which significantly increase the neutron components below about 100 MeV and can lead to increases on more than one order of magnitude for neutrons below about 10 MeV especially for landing sites on Mars regolith. The HZETRN modifications presented elsewhere by Clowdsley et al. [5] to include the back-scattered neutrons are in excellent agreement with Monte-Carlo codes; however, there are no measurements to-date to validate this code on the Mars surface.

The Mars atmosphere is largely CO_2, however, contains a small amount of other constituents [19, 20]. It is also of interest for improved understanding of the possible history of life on Mars to consider the evolution and possible changes of the Martian atmosphere and their impact on radiation effects for possible life in the past. Figure 3 makes predictions for several possible atmospheric conditions including a methane atmosphere or a mixed CO_2 and CH_4 atmosphere. The 100% CH_4 atmosphere is included for reference. Along with the vertical height of the atmosphere, the mass contribution of hydrogen makes the most significant modulation of the surface radiation environment. The relative contributions from non-hydrogen atoms has only a small effect on the charged-particles ob-

Journal : 411 Dispatch : 8-2-2007 Pages : 7
Article No. : 99 LE TYPESET
MS Code : 99 CP DISK

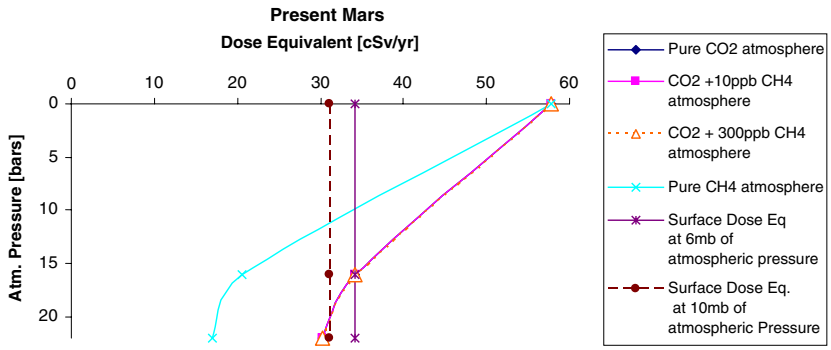

Fig. 3 Calculations of the dependence of the Mars surface point dose equivalent on atmospheric composition and density. Different atmospheric mixtures are shown including the temptative detection of methane (CH_4), which vary between 10 ppb (parts per billion) and a maximum of 300 ppb of CH_4. Two theoretical end cases of a pure CO_2 and pure CH_4 atmosphere are shown for reference

served on the Mars surface, however, are expected to have a slightly larger dependence for the albedo neutrons [5].

In summary, we have shown that the quantum multiple scattering model of nuclear fragmentation (QMSFRG) provides an accurate data base for GCR transport problem applications. It would be useful for additional fragmentation data to be obtained, including new data for Al and Ca fragmentation. Because the atmosphere of Mars represents one to two mean free paths for GCR heavy ions leading to buildup of light ion fragments, we have made predictions of the flux rates to be expected to be observed by RAD in 2010 for light and heavy particles, which include the nuclear coalescence contribution to the cross sections. Because the integral flux of GCR nuclei changes slowly with atmospheric parameters or geographical location of Mars, measurements of charge-specific energy spectra between 10 and 200 MeV/u are shown to provide the optimal tests of radiation transport codes. Future work will aim to improve the calculation of cross sections in the coalescence and cluster knockout models [8, 12], include the albedo neutron and light ion contributions, and describe detailed geometric models of the RAD configuration on MSL in preparation for the data analysis phase of the experiment.

Acknowledgment This work was sponsored, in-part, by the NASA Exploration Systems Management Directorates Space Radiation Research Programs Radiation Risk Assessment (F.A. Cucinotta) and Mars Science Laboratory Awards (D. Hassler).

References

1. Cucinotta FA, Durante M (2006) Cancer risks from exposures to galactic cosmic rays: implications for space exploration by human beings. Lancet Oncol 7:431–435
2. Cucinotta FA, Schimmerling W, Wilson JW, Peterson LE, Badhwar GD, Saganti P, Dicello JF (2001) Space radiation cancer risks and uncertainties for Mars missions. Radiat Res 156:682–688
3. Saganti PB, Cucinotta FA, Wilson JW, Simonsen LC, Zeitlin CJ (2004) Radiation climate map for analyzing risks to astronauts on the Mars surface from galactic cosmic rays. Space Sci Rev 110:143–156
4. Badhwar GB, Cucinotta FA, O'Neill PM (1994) An analysis of interplanetary space radiation exposure for various solar cycles. Radiat Res 138:201–208
5. Clowdsley M, Wilson JW, Kim MH, Singleterry RC, Tripathi, RK, Heinbockel JH, Badavi FF, Shinn JL (2001) Neutron environments on the Martian surface. Phys Medica XVII:94–96
6. Cucinotta FA, Townsend LW, Wilson JW (1992) Production of ^{3}H at large momentum in α-^{12}C collisions at 2A GeV. Phys Lett 282B:1–6
7. Cucinotta FA, Townsend LW, Wilson JW (1992) Multiple scattering effects in quasi-elastic α-^{4}He scattering. Phys Rev C 46:1451–1456
8. Cucinotta FA, Dubey RR (1994) Alpha cluster description of excitation energies in ^{12}C (^{12}C, 3 α) X at 2.1 GeV. Phys Rev C 50:979–984
9. Cucinotta FA et al (1997) Computational procedures and data-base development. In: Wilson JW, Miller J, Konradi A, Cucinotta FA (eds) NASA workshop on shielding strategies for human space exploration. NASA CP-3360
10. Cucinotta FA, Wilson JW, Townsend LW (1997) Abrasion–ablation model for neutron production in heavy ion collisions. Nucl Phys A 619:202–212
11. Campi X, Hufner J (1981) Nuclear spallation–fragmentation reactions induced by high-energy projectiles. Phys Rev C 24:2199–2209
12. Cucinotta FA (1994) Forward production of protons in relativistic ^{12}C-nucleus collisions. J Phys G Nucl Part Phys 20:1803–1815
13. Leupold S, Heinz U (1994) Coalescence model for deuterons and anti-deuterons in relativistic heavy–heavy ion collisions. Phys Rev C50:1110–1128
14. Wilson JW, Badavi FF (1986) Methods of galactic heavy ion transport. Radiat Res 108:231–237
15. Wilson JW, Townsend LW, Schimmerling W, Khandelwal GS, Khan F, Nealy JE, Cucinotta FA, Simonsen LC, Shinn JL, Norbury JW (1991) Transport methods and interactions for space radiations. NASA RP-1257

Journal : 411 | Dispatch : 8-2-2007 | Pages : 7
Article No. : 99 | LE | TYPESET
MS Code : 99 | CP | DISK

16. Cucinotta FA, Wilson JW, Saganti P, Hu X, Kim MY, Cleghorn T, Zeitlin C, Tripathi RK (2006) Isotopic dependence of GCR fluence behind shielding. Radiat Meas 41:1235–1249
17. Zeitlin C, Fukumura A, Guetersloh SB, Heilbronn LH, Iwata Y, Miller J, Murakami T (2006) Fragmentation cross sections of ^{28}Si at beam energies from 290 A to 1200 A MeV. Nucl Phys A (in press)
18. Olsen DL, Berman BL, Greiner DE, Heckman HH, Lindstrom PJ, Crawford HJ (1981) Factorization of fragment-production cross sections in relativistic heavy-ion collisions. Phys Rev C28:1602–1613
19. Krasnopolsky VA, Maillard JP, Owen TC (2004) Detection of methane in the martian atmosphere: evidence for life? Icarus 172:537–547
20. Formisano V, Atreya S, Encrenaz T, Ignatiev N, Giuranna M (2004) Detection of methane in the atmosphere of Mars. Science 306:1758–1761

Journal : 411 | Dispatch : 8-2-2007 | Pages : 7
Article No. : 99 | ☐ LE | ☐ TYPESET
MS Code : 99 | ☑ CP | ☑ DISK